AIAA JOURNAL
Vol. 42, No. 4, April 2004

Linear and Nonlinear Analysis of a Smart Beam Using General Electrothermoelastic Formulation

Sheikh N. Ahmad,* C. S. Upadhyay,† and C. Venkatesan‡
Indian Institute of Technology, Kanpur, Uttar Pradesh 208 016, India

Coupled electrothermoelastic equations applicable to the analysis of smart structures have been derived from first principles. Using the equations and applying a layer-by-layer finite element model, the induced potential and mechanical deformations in the piezo and nonpiezo core material have been obtained for various cases of actuation and sensing of a smart beam under external mechanical load and actuation potential. The present study clearly brings out the essential difference between sensing and actuation. It is also brought out that the interaction between polarization and electric field in the piezo continuum leads to nonlinear distributed body force and nonsymmetric stress tensor. These nonlinear effects are found to have significant influence on the deformation of a smart beam under actuation. Shape control studies of multipatch smart beams have also been investigated.

Nomenclature

b_{ij}	=	dielectric permittivity
C_{ijkl}	=	elastic constant
D_i	=	electric displacement
d_i	=	pyroelectric constant
E_i	=	electric field
e_{ijk}	=	piezoelectric constant
F	=	tip load or load vector
i, j, k, l	=	vary from 1 to 3 and designate respective components
k_{ij}	=	thermoelastic constant
$\boldsymbol{P}$	=	polarization vector
P_i	=	polarization per unit volume
q_i	=	heat flux
$\boldsymbol{r}$	=	position vector
s	=	entropy
u_i	=	displacement
α	=	heat capacity per unit reference temperature
ϵ_0	=	permittivity constant of free space
ϵ_{ij}	=	strain
η	=	dielectric susceptibility
θ	=	absolute temperature
θ_0	=	reference absolute temperature
σ_{ij}	=	nonsymmetric stress tensor, given as $\sigma_{ij} = \sigma_{ij}^S + \sigma_{ij}^A$
σ_{ij}^A	=	antisymmetric stress tensor, given as $\sigma_{ij}^A = \frac{1}{2}(E_i P_j - P_i E_j)$
σ_{ij}^S	=	symmetric stress tensor
ϕ	=	electric potential

I. Introduction

WITH the consolidation of composite materials for the construction of aerospace structures, enormous effort is currently being focused on the development of smart or intelligent structures. Under external loading, conventional structures deform in a passive manner with no control over the configuration of the deformed state. In contrast, in smart structures, the structural deformation is continuously monitored and controlled (using distributed sensors and actuators) to achieve the desired configuration of the deformed state of the structure. In principle, distributed sensing and actuation can be implemented by embedding piezoelectric material in the structure. Piezoelectricity represents the interaction between electrical and mechanical characteristics of a material. Though piezoelectric material was discovered by the Curie brothers in the 1880s, the potential for use in deformation control and health and usage monitoring of flexible structures is of recent origin.

In piezoelectric materials an electrical voltage is developed when mechanical loading (pressure) is applied. This is known as direct piezoelectric effect. In the indirect or converse effect, the piezoelectric materials undergo mechanical strain when a voltage is applied across them. The direct and converse effects form the fundamental basis for the use of piezoelectric materials, both as sensors and as strain actuators. The electroelastic characteristics of piezoelectric materials have been studied extensively by physicists and materials scientists. It is well established that the electrical properties of piezoelectric materials depend on temperature. In addition, under cyclic variation of electric field, material polarization exhibits a hysteresis effect leading to energy loss. The interaction among the three fundamental constituents, namely, mechanical, electrical, and thermal loading on piezoelectric materials, can best be described by the diagram shown in Fig. 1 (Refs. 1 and 2). The various interactions depicted in Fig. 1 show the complexity of the problem. Essentially three types of behavior exist in a piezoelectric crystal: thermoelasticity, piezoelectricity, and pyroelectricity. An electric field $\boldsymbol{E}$ causes piezoelctric stress $\sigma = e'\boldsymbol{E}$, where e' is the appropriate piezoelectric stress coefficient. Similarly a strain ϵ causes the electric polarization $\boldsymbol{P} = e\epsilon$. In a similar manner, the pyroelectric constant p relates a change in temperature ΔT with polarization $\boldsymbol{P}$; the arrow from $\boldsymbol{E}$ to δQ indicates the electrocaloric effect (i, e., the variation in the quantity of heat Q on application of an electric field $\boldsymbol{E}$), which is usually expressed as a relation between the change in temperature ΔT and $\boldsymbol{E}$. The thermal coefficient of expansion α relates ΔT to ϵ; the arrow from σ to ΔQ with a coefficient b relating them indicates the thermoelastic effect. Stress σ and strain ϵ are related by an equation of the form $\epsilon = s\sigma$. In an analogous manner, polarization $\boldsymbol{P}$ and electric field $\boldsymbol{E}$ are related by dielectric susceptibility η, and quantity of heat ΔQ is related to change in temperature ΔT through specific heat c. The arrows indicate the directions in which the various effects usually take place. The additional arrow between $\boldsymbol{P}$ and $\boldsymbol{E}$ indicates that an electric field may exist by virtue of polarization in the material.

Each of the nine straight lines in Fig. 1 usually represents the primary or "true" effect. However, in every case there is at least one other path over which the process can take place, unless the coefficients are zero for that particular process for the material (or crystal)

Received 29 January 2003; presented as Paper 2003-1637 at the 11th Adaptive Structures Conference, Norfolk, VA, 7–10 April 2003; revision received 4 December 2003; accepted for publication 5 December 2003.

*Graduate Student, Department of Aerospace Engineering.
†Assistant Professor, Department of Aerospace Engineering.
‡Professor, Department of Aerospace Engineering; cven@iitk.ac.in. Senior Member AIAA.

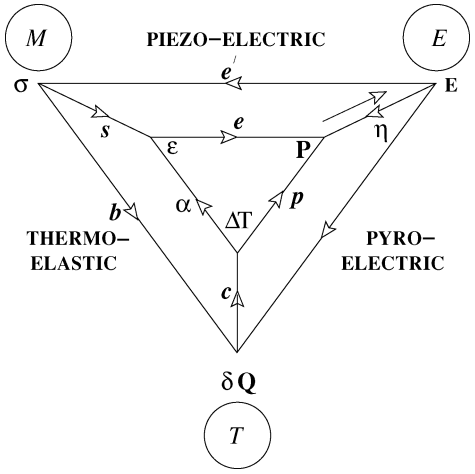

Fig. 1 Electrothermoelastic interaction.

under consideration. The roundabout effects are usually denoted as "false" or secondary effects. An example is the false pyroelectric effect due to piezoelectric action, which may be several times greater than the direct effect itself. The primary pyroelectric effect is indicated by the path $\Delta T \rightarrow \boldsymbol{P}$, whereas the secondary effect follows the path $\Delta T \rightarrow \epsilon \rightarrow \boldsymbol{P}$. The reason for this complication is that every pyroelectric crystal is also piezoelectric. Therefore a change in temperature of unconstrained crystal causes a deformation and this in turn produces secondary polarization of piezoelectric origin superposed on the primary pyroelectric polarization. Therefore it is evident that primary pyroelectricity would be observed only in a completely clamped crystal.

In a similar manner, when an elastic compliance coefficient s is measured by observations of σ and ϵ, piezoelectric polarization $\boldsymbol{P}$ is produced, which, if the crystal is not short-circuited, gives rise to an electric field $\boldsymbol{E}$, which in turn modifies the value of stress σ. In addition, through thermoelastic effect there is a change in temperature, which affects the value of strain ϵ. Hence it becomes important to specify the conditions under which the material coefficients are measured and they must be properly incorporated into the analysis of smart structures having a base structure with embedded piezo layers.

A survey of the literature on smart structures indicates that there are two distinct lines of research, namely, studies of the fundamental formulation of the constitutive and equilibrium laws applicable to structures subjected to thermal, electrical, and mechanical loading under the title of electrothermoelasticity.[3−6] and studies related to application of smart materials to static and dynamic control of structures, which usually assume the electroelastic laws in either the decoupled or coupled form.[7−24]

The first static electroelastic formulation was given by R. A. Toupin in 1956 and later by Eringen and Suhubi.[3] In this formulation the authors derived the governing equations based on variational principles. Later, Tiersten[4] derived the nonlinear governing equations of electrothermoelasticity by applying basic conservation laws of continuum physics to a macroscopic model. He assumed that the macroscopic model consisted of a material continuum having inertia and an electronic continuum without inertia, overlapping with each other. The equilibrium equations have been derived by balancing forces, when the electronic continuum is separated from the material continuum under external electric field. The constitutive equations are derived by applying the laws of thermodynamics and the appropriate boundary conditions are obtained using a variational formulation.

A comprehensive survey on smart technology can be found in Ref. 7. Zhang and Sun[8] have presented a theoretical formulation of an adaptive beam actuation problem in both extension mode (piezopatches on top and bottom of aluminum core) and shear mode (piezopatch sandwiched between aluminum layers). They derived governing electroelastic equations based on variational principles. They have shown that shear-mode actuation is advantageous over extension-mode actuation because piezoelectric material cannot sustain large axial stresses. Dube et al.[9] have analyzed the problem of a single-layer piezopanel under external mechanical, thermal, and electrical loadings. Effect of width-to-thickness ratio of piezopanel on the axial displacement, transverse displacement, and axial stress has been investigated. Chattopadhyay et al.[10] have presented a finite element formulation for coupled electrothermoelastic problem for smart composite plates under thermal loading using higher order displacement and temperature fields. They have studied the temperature variation in the composite stack for several lay-up sequences. It is shown that piezo actuation overpredicts the plate deformation in the uncoupled case relative to the coupled case. Aldraihem and Ahmed[11] have shown that there is a significant difference between the deflections obtained for the cases of first-order beam theory and higher order beam theory for the shear-mode actuation, whereas the difference is observed to be very small in the case of extension-mode actuation. Librescu et al.[12] have presented a dual approach integrating 1) composite tailoring and 2) adaptive materials technology to control the dynamic response of a closed-cell thin-walled wing structure subjected to external excitations. Nonclassical effects such as anisotropy, transverse shear, and warping restraint have also been introduced and their influence on the dynamic response of a cantilever structure has been studied. Crawley and Luis[13] have presented the analytic and experimental development of piezoelectric actuators as elements of a cantilever beam. The details of the preparation of smart beams have been clearly described. Several static and dynamic experiments have been conducted using different test specimens and correlated with the theoretical analysis. It is concluded that surface-mounted or embedded piezopatch segments can better control the deformation of the structure than continuous piezopatches because the influence of each piezopatch on the structural response can be individually controlled. Shen[14] has developed a beam model for the sensing and actuation of a smart beam having multiple piezopatches. The static and dynamic responses of the smart beam have been analyzed. Bengeddou et al.[15] have presented a finite element formulation for the analysis of adaptive sandwich beam for extension/shear actuation mechanisms. Based on the studies, he concluded that for stiff beams shear actuation is better than extension mode actuation. Robbins and Reddy[16] have presented a piezoelectrically actuated beam problem using layerwise displacement theory. Results of layerwise theory are compared with the conventional higher order shear deformation theory and the necessity of multilayer modeling for nonhomogeneous cross sections is brought out. Ha et al.[17] have presented a finite element analysis for modeling the electroelastic response of fiber-reinforced laminated composite plates and beams. Three-dimensional brick finite elements have been used for analysis. Theoretically obtained transverse deformations for beams and plates have been correlated with experimental results. Shih[18] has studied the distributed vibration sensing and control of a piezoelectric laminated curved beam. Parametric studies are carried out, and it is shown that distributed surface-bonded piezoelectric polymer layers can enhance the system damping and therefore effectively control the oscillation amplitude. Liu et al.[19] have presented a finite element formulation to model the static and dynamic response of laminated composite plates containing integrated piezoelectric sensors and actuators. The influence of stacking sequence and locations of sensors and actuators on the response of a composite plate have been evaluated. Sun and Huang[20] have presented analytical solutions of composite beams with piezoelectric laminae. Active vibration control of smart laminated beams under different frequencies of external exciting force has been investigated. In Ref. 21 Tzou and Howard have developed a generic piezothermoelastic shell theory for thin piezoelectric shells using linear piezoelectric theory. Mujumdar et al.[22] present the details of the experiments performed on smart beams and bimorph actuators. The static response of beam deformation has been measured for various actuation voltages. Chopra[23] has presented a comprehensive review on the status of the application of smart technology to rotorcraft.

In studies addressing the application of smart structures,[7−21] the key difference between actuation and sensing has not been clearly brought out. The essential difference between actuation and sensing is in identifying the contribution to the induced electric potential

across the piezopatch due to externally applied potential as well as to mechanical strain. In all of the studies addressing the application of smart materials to structures, certain fundamental assumptions have been made in using the following constitutive relations:

$$\begin{Bmatrix} \boldsymbol{\sigma} \\ \boldsymbol{D} \end{Bmatrix} = \begin{bmatrix} \bar{c} & \bar{e} \\ \bar{e} & \bar{\epsilon}^s \end{bmatrix} \begin{Bmatrix} \boldsymbol{\epsilon} \\ \boldsymbol{E} \end{Bmatrix}$$

where σ is the stress tensor, D is the electric displacement, ϵ is the strain, and E is the electric field in the piezo material. Most of the studies[8–13] have assumed that either the electric field is known to be uniform (i.e., $\boldsymbol{E}$ = voltage/thickness of piezopatch $= V/t$) along the direction of the applied voltage or a linear variation of electric potential, ϕ (along the direction of the applied voltage, i.e., z direction), in the form

$$\phi(x, z) = \phi_0 + z\phi_1$$

This assumption about the electric field $\boldsymbol{E}$ or electric potential ϕ essentially decouples the electric phenomenon from the elastic phenomena. In addition, the effect of material strain on the induced potential in the piezo material is completely neglected. (It may be noted that this assumption can be shown to be valid for certain special cases of actuation of smart structures using piezopatches but not for all situations. This important observation will be brought out in the present study on the actuation and sensing problem of a smart beam.)

In Refs. 14–16, the electric potential expression is modified to include the effect of material strain by first solving the electric displacement equilibrium equation ($D_{i,i} = 0$) in the transverse direction in an approximate manner. The improved (or modified) form of ϕ can be

$$\phi(x, z) = \phi_0 + z\phi_1 + cz^2 \frac{\mathrm{d}^2 w}{\mathrm{d}x^2}$$

where $\mathrm{d}^2 w/\mathrm{d}x^2$ is the bending curvature of the smart beam and c is a dimensional constant. This term is responsible for the induced potential developed in the piezo material due to straining. In addition this term acts as a coupling term between electric and elastic phenomenon of piezo materials. In the present study the electroelastic coupling is properly treated while the sensing and actuation of a smart beam are solved under external loading.

Moreover, to the best of the knowledge of the authors, in the studies addressing the application of smart materials to structures, no mention is made of 1) distributed nonlinear body force; 2) nonsymmetry of the stress tensor due to interaction of material polarization $\boldsymbol{P}$ and electric field $\boldsymbol{E}$; or 3) the requirement that $\boldsymbol{P}$ and $\boldsymbol{E}$ vectors must be parallel to make the stress tensor symmetric. The assumption of $\boldsymbol{P}$ and $\boldsymbol{E}$ vectors being parallel is valid for certain special cases of static problem. For the dynamic cases, this assumption is not valid because of strong hysteresis effect.

In this study, the electrothermoelastic equations applicable to static problems have been developed in a consistent manner. This formulation is used in bringing out the essential difference in actuation and sensing of a smart beam due to external mechanical loading and applied potential.

The objectives of the present study are 1) formulation of the governing equations for static coupled nonlinear electrothermoelasticity for a continuum model in a systematic manner; 2) development of a layer-by-layer finite element model for the actuation and sensing of a smart beam; 3) bringing out the essential difference between actuation and sensing behavior of the piezopatch of the smart beam under bending deformation; 4) carrying out a study on the shape control (or deformation control) of a multipatched smart cantilever beam; and 5) studying the effects of nonlinearities due to the interaction of polarization $\boldsymbol{P}$ and electric field $\boldsymbol{E}$ on the actuation of a smart beam.

II. Mathematical Formulation

The governing equations for electrothermoelasticity are derived by considering a single continuum having electrothermoelastic properties, essentially following the procedure outlined in Ref. 4.

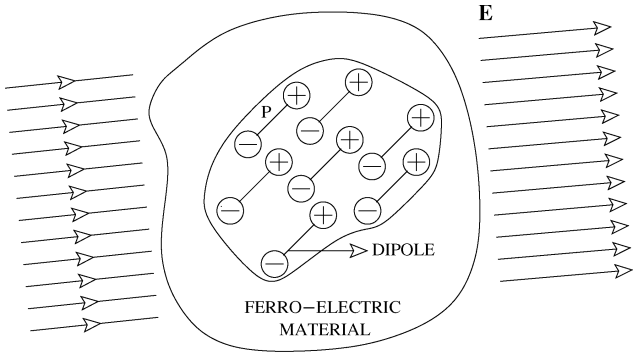

Fig. 2 Influence of electric field.

The mathematical formulation involves the development of three sets of equations, in a consistent manner. They are equilibrium equations, constitutive relations, and boundary conditions. On simplification, there are five equations in terms of five independent variables consisting of three displacements, one electric potential, and one temperature variable. The detailed formulation is presented in Ref. 24. A brief description of these equations is provided next.

A. Equilibrium Equations of Electrothermoelasticity

The development of electrothermoelastic formulation of smart structures is based on the following fundamental conservation laws: conservation of linear and angular momentum (force and moment equilibrium in the static case); conservation of charge; energy balance; and conservation of mass.

Let Ω_0 be the original, undeformed domain and let Ω be the deformed configuration of the body.

For an arbitrary volume element V, the external distributed forces and moments are (Fig. 2) force due to gravity: $\boldsymbol{f}$, force due to polarization of the medium $(\boldsymbol{P} \cdot \boldsymbol{\nabla})\boldsymbol{E}$, and moment due to polarization of the medium $\boldsymbol{P} \times \boldsymbol{E}$.

In the absence of free charges, the force and moment equilibrium in the deformed configuration can be written as

$$\int_V (\boldsymbol{f} + \{\boldsymbol{P} \cdot \boldsymbol{\nabla}\}\boldsymbol{E})\,\mathrm{d}V + \int_{\partial V} (\boldsymbol{\sigma} \cdot \boldsymbol{n})\,\mathrm{d}S = \frac{\mathrm{d}}{\mathrm{d}t} \int_V \rho \boldsymbol{u}\,\mathrm{d}V \tag{1}$$

$$\int_V \{\boldsymbol{r} \times (\boldsymbol{f} + \{\boldsymbol{P} \cdot \boldsymbol{\nabla}\}\boldsymbol{E}) + \boldsymbol{P} \times \boldsymbol{E}\}\,\mathrm{d}V + \int_{\partial V} \boldsymbol{r} \times (\boldsymbol{\sigma} \cdot \boldsymbol{n})\,\mathrm{d}S = \frac{\mathrm{d}}{\mathrm{d}t} \int_V \boldsymbol{r} \times \rho \boldsymbol{u}\,\mathrm{d}V \tag{2}$$

where V is an arbitrary portion of the domain Ω, and ∂V is the boundary of the portion V. It is assumed that the inherent mass moment of inertia per unit volume is zero. Further, assuming that the motion of the domain is quasi-static with respect to the electrical interactions, the charge conservation relationship for the portion V can be obtained as

$$\int_{\partial V} \boldsymbol{D} \cdot \boldsymbol{n}\,\mathrm{d}S = 0 \tag{3}$$

Equation (1) is rewritten in pointwise form as

$$\sigma_{ij,i} + E_{j,i} P_i + f_j = \rho \frac{\mathrm{d}u_j}{\mathrm{d}t} \tag{4}$$

The conservation of angular momentum (Eq. (2)) gives $\sigma_{ij}^A = \frac{1}{2}(E_i P_j - P_i E_j)$ with the Cauchy stress $\sigma_{ij} = \sigma_{ij}^S + \sigma_{ij}^A$. Note that the antisymmetric part of the stress tensor is completely defined in terms of the pointwise polarization and the electric field. Generally, in the application of piezoelectricity, the stress tensor is assumed to be symmetric, which means that the distributed moment

due to polarization is neglected. (The polarization is assumed to be aligned with the local electric field.)

The charge conservation can be written as

$$D_{i,i} = 0 \tag{5}$$

Because the electric field is irrotational, it can be expressed in terms of the derivative of a scalar potential(ϕ), as $E_i = -\partial\phi/\partial x_i$. Assuming quasi-static deformation without heat generation, the thermal equilibrium equation is

$$q_{i,i} = 0 \tag{6}$$

B. Constitutive Equations

Using a generalized thermodynamic potential and Clausius–Duhem inequality (second law of thermodynamics), the following constitutive relations are obtained:

$$\sigma_{ij} = C_{ijkl}\epsilon_{kl} - e_{ijk}E_k - k_{ij}\theta - P_i E_j \tag{7}$$

$$D_i = e_{ijk}\epsilon_{jk} + b_{ij}E_j + \mathrm{d}_i\theta \tag{8}$$

$$s = k_{ij}\epsilon_{ij} + \mathrm{d}_i E_i + \alpha\theta \tag{9}$$

$$\boldsymbol{D} = \epsilon_0 \boldsymbol{E} + \boldsymbol{P} \tag{10}$$

The details of the mathematical formulation can be found in Refs. 4 and 24.

C. Generalized Variational Formulation

The finite element formulation is based on using the variational principle. The variational form of the static electrothermoelastic formulation (neglecting gravity force) can be written as

$$\int_V (\sigma_{ij,i} + P_i E_{j,i})\delta u_j \,\mathrm{d}V + \int_V D_{i,i}\delta\phi \,\mathrm{d}V + \frac{1}{\theta_0}\int_V q_{i,i}\delta\theta \,\mathrm{d}V = 0 \tag{11}$$

In Eq. (11) the integral term $\int_V (P_i E_{j,i})\delta u_j \,\mathrm{d}V$ represents virtual work due to distributed force and σ_{ij} is nonsymmetric stress tensor and is given as

$$\sigma_{ij} = \sigma_{ij}^L + \sigma_{ij}^{NL} \tag{12}$$

The linear and nonlinear parts of the stress tensor are given, respectively, as $\sigma_{ij}^L = C_{ijkl}\epsilon_{kl} - e_{ijk}E_k - k_{ij}\theta$ and $\sigma_{ij}^{NL} = -P_i E_j$. Using the Gauss divergence theorem, Eq. (11) can be written as

$$\int_V \sigma_{ij}^L \delta\epsilon_{ij} \,\mathrm{d}V - \int_V D_i \delta E_i \,\mathrm{d}V + \frac{1}{\theta_0}\int_V q_i \delta\theta_{,i} \,\mathrm{d}V - \underline{\int_V (P_i E_{j,i})\delta u_j \,\mathrm{d}V} - \underline{\int_V P_i E_j \delta u_{j,i} \,\mathrm{d}V} = \int_S T_j \delta u_j \,\mathrm{d}S + \int_S Q\delta\phi \,\mathrm{d}S + \frac{1}{\theta_0}\int_S q_n \delta\theta \,\mathrm{d}S \tag{13}$$

where S represents the surface of the continuum and T_i refers to the components of mechanical traction force; Q is the electrical charge applied on the surface S of the piezo actuator; and q_n is the normal heat flux component. It may be noted that on a free surface, either the charge density Q is zero or the variation of the applied electric potential is zero. Therefore for any surface of a dielectric, the second integral on the right-hand side of Eq. (13) is always zero.

Specializing for a linear electroelastic problem by assuming that the nonlinear body force due to polarization is negligible and the distributed couple $\boldsymbol{P} \times \boldsymbol{E}$ is zero, Eq. (13) results in

$$\int_V \sigma_{ij}^L \delta\epsilon_{ij} \,\mathrm{d}V - \int_V D_i \delta E_i \,\mathrm{d}V = \int_S T_i \delta u_i \,\mathrm{d}S \tag{14}$$

D. Continuity Conditions

The boundary conditions are obtained by applying the integral form of the field equations [Eqs. (7–9)] to a pillbox region surrounding the surface of discontinuity. These boundary conditions in symbolic form are given as follows:

1) $[y_i] = 0$, displacement continuity
2) $[\phi] = 0$, potential continuity
3) $[\theta] = 0$, temperature continuity
4) $n_i[q_i] = 0$, heat flux continuity

The symbol [ ] indicates the jump in the values across material or domain interfaces.

III. Beam Model

In the present study on the actuation and sensing of a smart beam (Fig. 3), PZT-5H material has been chosen for the piezopatch. The material properties are given in Table 1. The constitutive model is transversely isotropic for the piezopatch. Aluminum is chosen as the core material for the smart cantilever beam and hence the constitutive relation for the core is isotropic. In the global coordinate system for describing the smart cantilever beam, x is along the longitudinal direction, z is along the thickness direction, and y completes the right-hand system as shown in Fig. 3. The constitutive linear relationship for PZT-5H (Ref. 8) is given as

$$\begin{Bmatrix} D_1 \\ D_2 \\ D_3 \\ \sigma_1 \\ \sigma_2 \\ \sigma_3 \\ \sigma_4 \\ \sigma_5 \\ \sigma_6 \end{Bmatrix} = \begin{bmatrix} \epsilon_1^s & 0 & 0 & 0 & 0 & 0 & 0 & e_{15} & 0 \\ 0 & \epsilon_1^s & 0 & 0 & 0 & 0 & e_{15} & 0 & 0 \\ 0 & 0 & \epsilon_3^s & e_{31} & e_{31} & e_{33} & 0 & 0 & 0 \\ 0 & 0 & -e_{31} & c_{11}^E & c_{12}^E & c_{13}^E & 0 & 0 & 0 \\ 0 & 0 & -e_{31} & c_{12}^E & c_{11}^E & c_{13}^E & 0 & 0 & 0 \\ 0 & 0 & -e_{33} & c_{13}^E & c_{13}^E & c_{33}^E & 0 & 0 & 0 \\ 0 & -e_{15} & 0 & 0 & 0 & 0 & c_{44}^E & 0 & 0 \\ -e_{15} & 0 & 0 & 0 & 0 & 0 & 0 & c_{44}^E & 0 \\ 0 & 0 & 0 & 0 & 0 & 0 & 0 & 0 & c_{66}^E \end{bmatrix} \times \begin{Bmatrix} E_1 \\ E_2 \\ E_3 \\ \epsilon_1 \\ \epsilon_2 \\ \epsilon_3 \\ \epsilon_4 \\ \epsilon_5 \\ \epsilon_6 \end{Bmatrix} \tag{15}$$

Table 1 Material properties of PZT-5H and aluminum

PZT-5H, GPa					PZT-5H, cm^{-2}			Al, GPa	
C_{11}^E	C_{12}^E	C_{13}^E	C_{33}^E	C_{44}^E	e_{31}	e_{33}	e_{15}	E	υ
126	79.5	84.1	117	23	−6.5	23.3	17.0	70.3	0.345

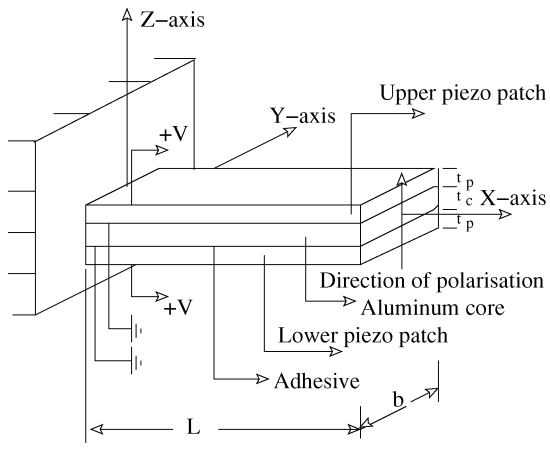

Fig. 3 Smart beam with full piezopatches.

The subscripts 1, 2, 3, 4, 5, and 6 refer to x, y, z, yz, xz, and xy, respectively. The poling direction of the piezopatches is along the z direction. D_i, E_i, σ_k, and ϵ_k refer to electric displacement components, electric field components, stress tensor, and linear strain tensor. ϵ_i^s, e_{ij}, and c_{ij}^E refer to the dielectric permittivity tensor at constant strain, the components of piezoelectric constants, and the elastic constants at constant electric field, respectively. Each layer of the beam is assumed to be in a state of plane strain in the x–z plane with normal stress in the z direction equal to zero. The interface between different material layers is assumed to be perfectly bonded.

A. Reduced Constitutive Relations

By imposing the conditions that $\gamma_{yz} = \gamma_{xy} = \epsilon_y = 0$ and $\sigma_z = 0$ in each layer, the reduced constitutive relations can be obtained as

$$\sigma_x = c^* \epsilon_x - e^* E_z \tag{16}$$

$$\sigma_{xz} = -e_{15} E_x + c_{44} \gamma_{xz} \tag{17}$$

$$D_x = \epsilon_1^s E_x + e_{15} \gamma_{xz} \tag{18}$$

$$D_y = \epsilon_1^s E_y + e_{15} \gamma_{yz} \tag{19}$$

$$D_z = \epsilon_3^* E_z + e^* \epsilon_x \tag{20}$$

where $c^* = (c_{11} - c_{13}^2/c_{33})$ (for both piezo and nonpiezo material), $e^* = [e_{31} - (c_{13}/c_{33}) e_{33}]$, and $\epsilon_3^* = (\epsilon_3^s + e_{33}^2/c_{33})$ (for piezo material only).

B. Displacement and Electric Potential Fields

The variables considered for the smart beam analysis are the displacements (u, v, w) in the core as well as in the piezo material and an electric potential ϕ in the piezo material. The axial displacement u is assumed to be a cubic function of z and x for both the core and the piezopatches. The cubic variation of axial displacement along z is used for implementing higher order beam bending theory. The electric potential is assumed to be a cubic function of x and a quadratic function of z so that the strain-induced potential can be properly modeled in the piezopatches. In each layer, the displacement fields are assumed to be

$$\bar{u}(x, y, z) = u(x, z) = \sum_{i=0}^{3} z^i u_i(x) \tag{21}$$

$$\bar{v}(x, y, z) = 0 \tag{22}$$

$$\bar{w}(x, y, z) = w(x) = w_0(x) \tag{23}$$

The electric potential variation in the piezo material is

$$\bar{\phi}(x, y, z) = \phi(x, z) = \phi_0(x) + z\phi_1(x) + z^2 \phi_2(x) \tag{24}$$

Respectively, $\bar{u}(x, y, z)$, $\bar{v}(x, y, z)$, and $\bar{w}(x, y, z)$ refer to global displacement variation along x, y, and z.

C. Global and Local Coordinates

Coordinate z in the global system can be transformed to the local $\bar{z}$ coordinate using the transformation, $z = \bar{z} + z_0$. Therefore one can write Eq. (24) as

$$\phi(x, \bar{z}) = \left(\phi_0(x) + z_0\phi_1(x) + z_0^2 \phi_2(x)\right) + \bar{z}(\phi_1(x) + 2z_0\phi_2(x)) + \bar{z}^2 \phi_2(x) \tag{25}$$

where $\bar{z}$ refers to the local coordinate in a particular layer and z_0 refers to the distance from the middle of the beam up to the middle of a layer,

$$\phi(x, \bar{z}) = \bar{\phi}_0(x) + \bar{z}\bar{\phi}_1(x) + \bar{z}^2 \bar{\phi}_2(x) \tag{26}$$

Though Eq. (26) appears similar to Eq. (24), it brings out the difference between the local and global coordinates. Following a similar procedure, axial displacement u can be written as

$$u(x, \bar{z}) = \bar{u}_0(x) + \bar{z}\bar{u}_1(x) + \bar{z}^2 \bar{u}_2(x) + \bar{z}^3 \bar{u}_3(x) \tag{27}$$

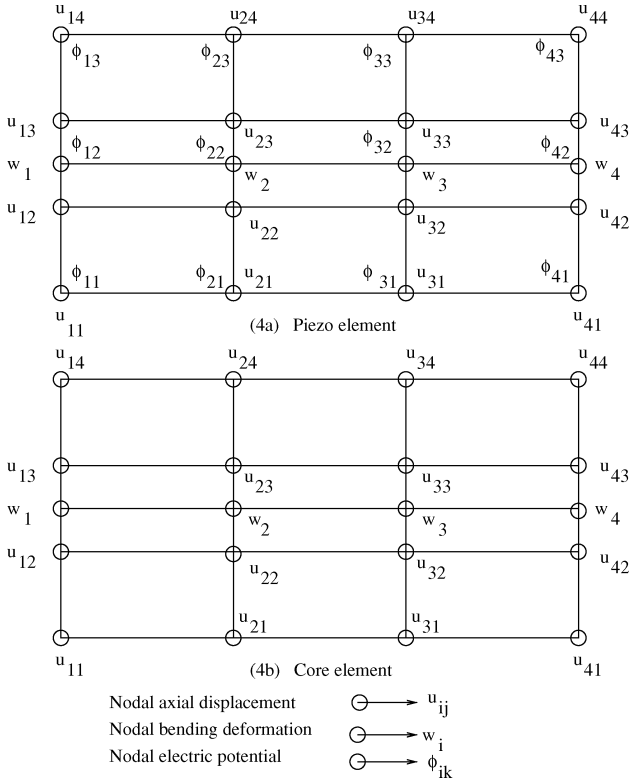

Fig. 4 Finite element nodal degrees of freedom.

It is evident from these transformations that $\bar{z}$ can henceforth be replaced by z without loss of clarity.

D. Finite Element Formulation

The element used for modeling the piezopatch, shown in Fig. 4a, has four nodes. Each node has eight degrees of freedom. These correspond to four axial displacements in the thickness direction, one transverse displacement, and three electric potentials along the thickness direction. This results in a stiffness matrix on the order of 32×32 for the piezopatch element, whereas the element for the nonpiezo core material (Fig. 4b), has four nodes, having five degrees of freedom per node. These correspond to four axial degrees of freedom in the thickness direction and one transverse displacement. This results in a stiffness matrix on the order of 20×20 for the nonpiezo core element.

1. Linear Analysis

Assuming that the smart cantilever beam is acted on by a tip load F, the variational expression given in Eq. (14) becomes

$$\int_V (\sigma_x \delta\epsilon_x + \sigma_{xz} \delta\gamma_{xz})\, \mathrm{d}V - \int_V (D_x \delta E_x + D_z \delta E_z)\, \mathrm{d}V = F \delta w \,|_{x=L} \tag{28}$$

Using the reduced constitutive relations Eqs. (16)–(20) and substituting $E_i = -\partial\phi/\partial x_i$, Eq. (28) can be written as

$$\int_V \left\{ \left(c^* \epsilon_x - e^* \left(\frac{-\partial\phi}{\partial z} \right) \right) \delta\epsilon_x + \left(-e_{15} \left(\frac{-\partial\phi}{\partial x} \right) + c_{44} \gamma_{xz} \right) \delta\gamma_{xz} \right\} \mathrm{d}V - \int_V \left\{ \left(\epsilon_1^s \left(\frac{-\partial\phi}{\partial x} \right) + e_{15} \gamma_{xz} \right) \delta \left(\frac{-\partial\phi}{\partial x} \right) + \left(\epsilon_3^* \left(\frac{-\partial\phi}{\partial z} \right) + e^* \epsilon_x \right) \delta \left(\frac{-\partial\phi}{\partial z} \right) \right\} \mathrm{d}V = F \delta w \,|_{x=L} \tag{29}$$

The axial and transverse displacements are given in the discretized form as

$$u(x, z) = \sum_{i=1}^{4} N_i(z) \bar{u}_i(x) \tag{30}$$

where

$$\bar{u}_i(x) = \sum_{j=1}^{4} u_{ij} N_j(x), \qquad i = 1, 2, \ldots, 4$$

$$w(x, z) = w(x) = \sum_{i=1}^{4} N_i(x) w_i \tag{31}$$

where

$$N_1(\xi) = -(9/16)(\xi + 1/3)(\xi - 1/3)(\xi - 1)$$

$$N_2(\xi) = (27/16)(\xi + 1)(\xi - 1/3)(\xi - 1)$$

$$N_3(\xi) = -(27/16)(\xi + 1)(\xi + 1/3)(\xi - 1)$$

$$N_4(\xi) = (9/16)(\xi + 1)(\xi + 1/3)(\xi - 1/3)$$

The electric potential is given in the discretized form as

$$\phi(x, z) = \sum_{i=1}^{3} F_i(z) \bar{\phi}_i(x) \tag{32}$$

where

$$\bar{\phi}_i(x) = \sum_{j=1}^{4} \phi_{ij} N_j(x)$$

and the quadratic interpolation functions in natural coordinate ξ are given as

$$F_1(\xi) = \tfrac{1}{2}\xi(\xi - 1)$$

$$F_2(\xi) = -(\xi - 1)(\xi + 1)$$

$$F_3(\xi) = \tfrac{1}{2}\xi(\xi + 1)$$

Substituting Eqs. (30), (31) and (32) into Eq. (29), the elemental stiffness matrix for piezo material can be written symbolically as

$$\begin{bmatrix} \left[K_{11}^{\text{elastic}}\right]_{20\times 20} & \left[K_{12}^{\text{electroelastic}}\right]_{20\times 12} \\ \left[K_{12}^{\text{electroelastic}}\right]_{12\times 20} & \left[K_{22}^{\text{electric}}\right]_{12\times 12} \end{bmatrix}$$

The vector of degrees of freedom for the piezo material element is given as

$$\begin{Bmatrix} \begin{Bmatrix} \{u\}_{4\times 1} \\ \{w\}_{1\times 1} \end{Bmatrix}_{4\times 1} \\ \{\phi\}_{12\times 1} \end{Bmatrix}_{32\times 1}$$

Therefore the discretized static linear electoelastic equilibrium equation for the entire smart beam can be written as

$$[K]\{a\} = \{F\} \tag{33}$$

where $[K]$ is the global stiffness matrix, $\{a\}$ is the vector of global degrees of freedom, and $\{F\}$ is the global load vector.

2. Nonlinear Analysis

Inclusion of nonlinear terms due to the interaction of $\boldsymbol{P}$ and $\boldsymbol{E}$ (underlined terms in Eq. (13)) requires the relation between $\boldsymbol{P}$ and $\boldsymbol{E}$, which is obtained using Eqs. (8) and (10). Assuming $E_y = 0$, $\partial E_x/\partial y = 0$, $\partial E_y/\partial y = 0$, $\partial E_z/\partial y = 0$, $\partial E_y/\partial z = 0$, $\partial E_y/\partial x = 0$, and $\delta(\partial v/\partial x) = \delta(\partial v/\partial y) = \delta(\partial v/\partial z) = 0$, the static nonlinear electroelastic equilibrium equation is formulated which can be symbolically written as

$$[K]\{a\} + [K_1(u, w, \phi)]\{a\} + [K_2(u, w, \phi)]\{a\} = \{F\} \tag{34}$$

where $[K_1(u, w, \phi)]$ and $[K_2(u, w, \phi)]$ represent the nonlinear extended stiffness matrices due to distributed force and moment terms, respectively.

IV. Results and Discussion

Using the formulation developed, several studies have been carried out. First, using the linear electroelastic formulation, the problems of actuation, sensing, and deformation control of a smart beam having single or multiple piezopatches have been analyzed. The results of these studies are presented in the following three sections, namely, 1) actuation, 2) sensing, and 3) shape control. Next the influence of nonlinear terms on the actuation of the smart beam has been studied.

A. Actuation

First, a coupled electroelastic problem is solved to validate the mathematical formulation and the solution procedure. The problem chosen for this case is surface-mounted actuation of a smart beam, as shown in Fig. 3. The polarization axis of the piezopatch is along the z direction and the external potential is also applied across the z direction. The properties for piezo and aluminum materials are given in Table 1. The beam consists of an aluminum inner core with two piezopatches on the top and bottom surfaces. The length of the beam is 100 mm having unit width. The aluminum-core thickness is 16 mm, and the PZT-5H piezopatch thickness is 1mm. The variation of bending deformation under an actuation voltage of 10 V has been evaluated and the results are compared with Ref. 8.

Figure 5 shows a comparison of the present results with those of Ref. 8. The results indicate that the present calculation shows a tip deflection 7.2% higher than that found by Zhang and Sun.[8] The reason can be attributed to the assumptions made by Ref. 8. They have assumed Euler–Bernoulli beam bending in piezopatches and Timoshenko beam theory in the core, whereas in the present study higher order beam bending in both core and piezopatches is taken. In addition, Ref. 8 assumes that the electric field is uniform across the thickness of the piezopatch and is equal to V/t, whereas in the present study the effect of strain on the electric field in the piezopatch is included. In a preliminary study, Ref. 25, the authors have reproduced the results of Ref. 8 by making assumptions identical to those of Ref. 8.

Next, the effect of variation of core thickness of the smart beam on the tip deflection and the potential developed at the midlayer of the piezopatch is studied, using the same smart beam model shown in Fig. 3. The thickness of the piezopatch is 1 mm and the actuation voltage across the patch in the z direction is taken as 10 V for all cases. Figure 6 shows the variation of tip deflection with core thickness. It can be seen that as the core thickness is reduced the tip deflection increases. Table 2 shows the potential developed at the mid layer of the piezopatch along the span at various nodal points. The free surface and the interface voltages in the piezopatch are 10 and 0 V, respectively. As the core thickness is reduced, the voltage at the midlayer increases monotonically. The results of the present study indicate that the assumption of uniform electric field is not valid as the core thickness is reduced. The reason for the difference in the midlayer voltage (from 5 V) is due to combined effect of applied potential and the induced potential due to straining. For the same actuation voltage (10 V), as the core thickness is reduced, the beam undergoes large strain, resulting in an increase in the induced potential in piezopatch. For a core thickness of 16 mm, the potential

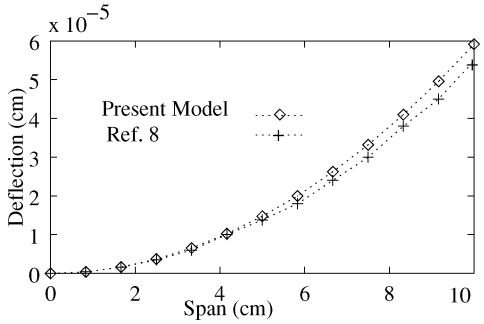

Fig. 5 Transverse deflection along the span of the smart beam actuated with 10 V.

Table 2 Variation of electric potential at midlayer of the piezopatch with core thickness of smart beam under 10 V actuation[a]

Location	Free surface applied voltage, V	Induced potential at midlayer (V) for core thickness: 16 mm	5 mm	2 mm	1 mm	Interface potential, V
Root	10.0	5.0198 (0.394%)	5.1193 (2.33%)	5.3209 (6.03%)	5.5003 (9.095%)	0.0
↓	10.0	5.0193 (0.384%)	5.1190 (2.324%)	5.3208 (6.029%)	5.5004 (9.097%)	0.0
↓	10.0	5.0197 (0.392%)	5.1192 (2.328%)	5.3208 (6.029%)	5.5003 (9.095%)	0.0
Mid span	10.0	5.0161 (0.32%)	5.1171 (2.228%)	5.3207 (6.027%)	5.5011 (9.109%)	0.0
↓	10.0	5.0204 (0.406%)	5.1198 (2.339%)	5.3209 (6.03%)	5.5001 (9.092%)	0.0
↓	10.0	5.0156 (0.311%)	5.1173 (2.292%)	5.3208 (6.029%)	5.5010 (9.107%)	0.0
Tip	10.0	5.0651 (1.285%)	5.1421 (2.762%)	5.3218 (6.046%)	5.4924 (8.965%)	0.0

[a]Percentage quantities represent the difference between uniform electric field assumption and the present study.

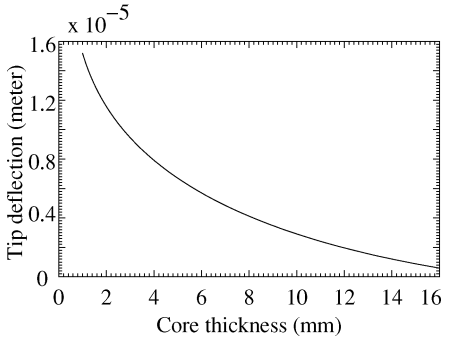

Fig. 6 Variation of tip deflection with core thickness of smart beam for 10-V actuation.

in the midlayer varies from 5.0198 V at the root to 5.0651 V at the tip. But for a core thickness of 1 mm, the potential in the midlayer is around 5.5 V, whereas the assumption of uniform electric field ($V = Et$) will provide 5 V at the midlayer.

B. Sensing

The sensing problem of a smart beam under the application of external mechanical load is solved for single-patched and multipatched smart beams.

1. Single-Patch Sensing

In solving the sensing problem, three different cases of electrical boundary conditions have been considered. These are as follows:

1) A single point (either at the fixed end or at the midpoint or tip) of the piezopatch on the interface is assumed to have zero potential (grounded).

2) The entire interface of the piezopatch is assumed to have zero potential.

3) The entire interface of the piezopatch is at zero potential and the free surface is at equipotential.

For the sake of comparison, the beam parameters are kept the same as in the single-patch actuation case. The results of the sensing problem of a smart beam (Fig. 3) are shown in Figs. 7–11. Assuming a tip deflection of 5.91402×10^{-7} m (note that this deflection is corresponding to the tip deflection of the smart beam, core thickness = 16 mm, at 10-V actuation as shown in Fig. 5), the induced potential in the free surface, the interface, and the middle layers of a piezopatch were evaluated. It is observed that the potential difference between the free surface and interface in the piezopatch is found to vary in the range from 0.0 to 2 V along the span of the beam. This voltage is much smaller than the 10 V required to produce the same tip deflection in the actuation case. The reason for this marked difference between sensing and actuation lies in the physical phenomenon of induced potential in the piezopatch under the action of externally applied potential and mechanical straining.

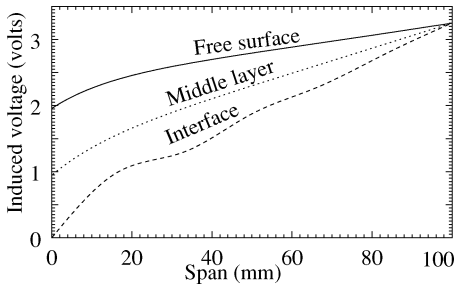

Fig. 7 Case 1: root end (single point) of interface is at zero potential.

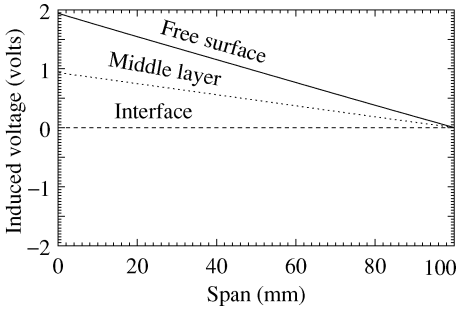

Fig. 8 Case 2: interface of the piezopatch at zero potential.

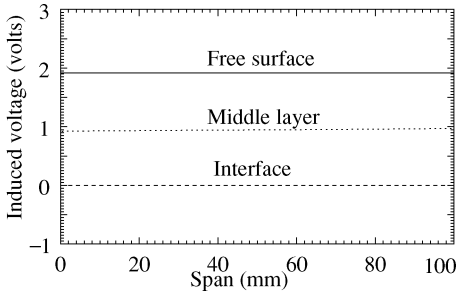

Fig. 9 Case 3: grounded interface and equipotential free surface.

Figure 7 shows the variation of induced potential along the span at the free surface, middle layer, and interface of the top piezopatch of the beam for case 1. At the root the voltages induced at the interface, midlayer, and free surface are 0, 1, and 2 V, respectively. It is clear that the potential difference across the thickness is maximum at the root and zero at the tip, indicating that induced strain is maximal at

Table 3 Comparison of sensed voltages for a multipatch smart cantilever beam

	Voltages induced for piezopatch:					
Study	1	2	3	4	5	6
Expt.[14]	11.25 V	8.90 V	7.25 V	NA	NA	NA
Analysis[14]	10.98 V	9.04 V	7.1 V	5.15 V	3.2 V	1.26 V
Present	11.16 V	9.26 V	7.36 V	5.45 V	3.55 V	1.65 V

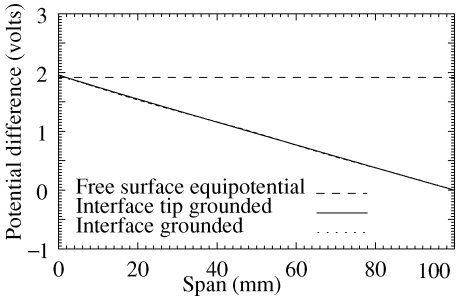

Fig. 10 Induced potential difference along the span.

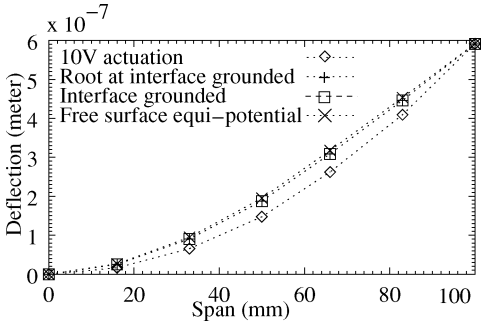

Fig. 11 Transverse deflection along span of the smart beam for 10-V actuation and for different cases of sensing.

the root and zero at the tip. A similar result is also observed for the bottom piezopatch of the beam.

For case 2, the variation of induced potential difference along the span is almost linear, having a maximum value at the root and zero at the tip, as shown in Fig. 8. For case 3, the potential difference is constant along the beam, with a value of about 2 V along the span, as shown in Fig. 9.

Figure 10 shows the variation of potential difference in the piezopatch along the span for three different cases. It is clear that for cases 1 and 2, the potential difference along the span is almost identical with a maximum value of about 2 V at root and zero at tip. The monotonically decreasing trend in the potential difference from the root to the tip has been experimentally observed in the case of multipatch sensing of a smart beam in Ref. 14. For case 3, the potential difference has a constant value of about 2 V along the span.

Figure 11 shows the bending deformation of the beam along the span for all cases. It can be seen that even though the tip deflection is identical, the deformation shape for sensing cases is different from that of the actuation case. Even among the three different sensing cases, there is a slight difference between the deformed configurations.

2. Multipatch Sensing

Figure 12 shows a multipatched smart cantilever having six pairs of piezopatches. The axis of polarization in the patches is in the z direction. For a tip deflection of 4.7625×10^{-3} m, voltages sensed in the six patches are calculated and they are shown in Table 3. Each patch is constrained to have zero potential at the interface and equipotential at the free surface.

The computed values of the sensed voltages in the six patches are in close agreement with the experimental and theoretical results

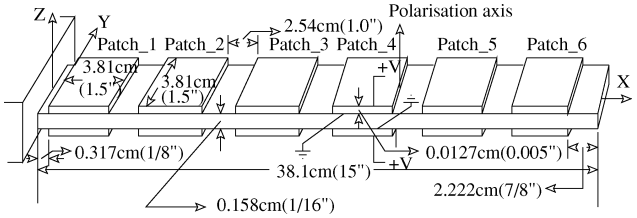

Fig. 12 Multipatch smart beam.

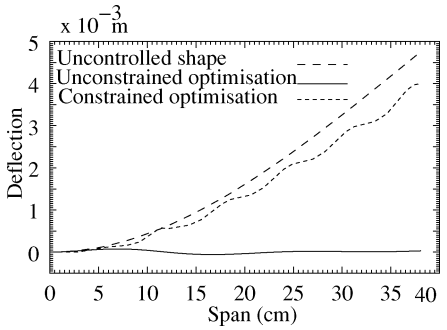

Fig. 13 Comparison of uncontrolled and controlled bending deformation of the beam.

given in Ref. 14. The results show that the voltages induced in the six patches decrease monotonically from a value of 11.16 V (for patch 1 at root) to 1.65 V (for patch 6 at tip). This variation in the induced potential is consistent with the variation in induced potential obtained for a single patch spanning the whole beam (with zero potential at interface and no voltage constraint at the free surface).

C. Shape Control

Using the multipatched beam model shown in Fig. 12, an open-loop shape control (bending deformation control) of the beam under a tip load was studied. The control variables of the problem are the six voltages to be applied across the six patches. The control variables have been obtained by minimizing an objective function

$$f = \sum_{i=1}^{NN} |w_i|^2$$

where w_i is the nondimensional bending displacement of the beam at the ith node. Under a tip load of 0.448 N, the uncontrolled deflection of the beam (having a tip deflection of 4.7625×10^{-3} m) is shown in Fig. 13.

Shape control studies have been carried out for both unconstrained and constrained cases. In the unconstrained case, there is no restriction on the actuator voltages in the six pairs of piezopatches. In the constrained case, the operating voltage is set below 1000 V/mm for voltage along the polarization axis and 550 V/mm in the opposite direction of polarization axis.

The uncontrolled and the controlled deformation of the beam are shown in Fig. 13. It can be seen that the controlled deformation of the beam is almost straight for the case of unconstrained actuation, whereas for the case of constrained optimization, the deformation control of the beam is not very effective. The voltages applied across piezopatches for the constrained and unconstrained minimization are shown in Table 4. It can be seen that the voltage required for constrained minimization is one order of magnitude less than that for the constrained case. The minimized value of the objective function for the unconstrained case is 1.324×10^{-3}, whereas for the constrained case it is 1.178.

The variation of the objective function for the unconstrained case is shown in Fig. 14, which shows a very good convergence. The magnified shape of the controlled beam is shown in Fig. 15. It is interesting to note that the control voltages deform the beam in alternate directions.

Table 4 Control voltages in six patches and objective function values

Optimization case	Control voltage V1	V2	V3	V4	V5	V6	Objective function
Unconstrained	80.3	428.4	−144.0	228.8	50.5	−4.7	1.32404×10^{-3}
Constrained	−58.1	−52.0	−60.0	−30.6	−60.0	9.3	1.1782

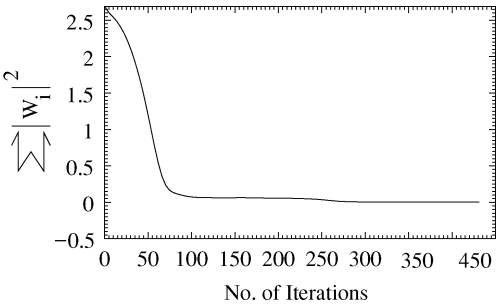

Fig. 14 Variation of objective function with iteration number (unconstrained case).

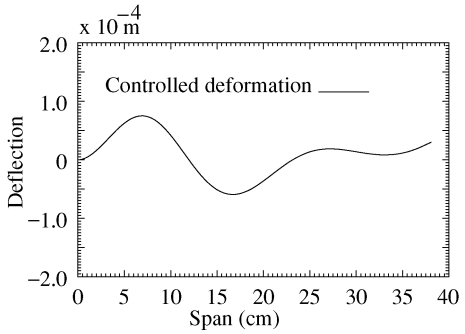

Fig. 15 Controlled bending deformation of the beam in magnified form (unconstrained case).

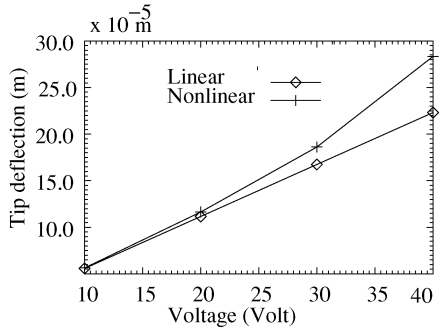

Fig. 16 Tip deflection as a function of actuation voltage.

D. Nonlinear Analysis

The example problem chosen for nonlinear analysis is shown in Fig. 3. The core thickness is 1.58 mm, the piezopatch thickness is 0.127 mm, and the beam length is 100 mm with unit width. The deformation of the beam is evaluated for various actuation voltages from 10 to 40 V in increments of 10 V. The tip deflection of the beam for the linear and the nonlinear cases is plotted as a function of applied voltage in Fig. 16. It can be seen that the tip deformation of the beam for the nonlinear case is higher than that in the linear case and the difference increases with increase in actuation voltage. The percentage difference between linear and nonlinear cases is on the order of 1.0% for 10-V actuation and increases to 21.24% for 40-V actuation. The reason for the significant difference observed for higher actuation voltage may be attributed to the increased influence of the distributed nonlinear moment and body force (due to the inclination of polarization and electric field vectors) on the deformation of the beam.

V. Conclusions

A general electrothermoelastic formulation has been developed from conservation laws and thermodynamic principles. The purpose of developing the general formulation of electrothermoelasticity is to address the physics of the problem in totality, and the formulation could be useful for further studies on this topic. In this paper the formulation has been specialized to address the electroelastic problem of a smart beam. Using a layer-by-layer finite element model, the deformation of a smart beam has been analyzed for actuation and sensing cases by solving both the linear and nonlinear coupled electroelastic problems. The important observations of the study are as follows:

1) For actuation of smart beams, the assumption of uniform electric field in the piezoactuator is found to be violated as the strain in the piezopatch increases.

2) The induced potential for sensing cases is shown to be proportional to the strain in the piezopatch. As a result the induced potential decreases monotonically from the root to the tip of a smart cantilever beam subjected to a tip load.

3) Multiple piezopatches can be effectively used to control the shape of a smart beam under external mechanical loading.

4) Nonlinear distributed force and couple existing due to the interaction between polarization and electric field vectors affect the deflection and the effect is more pronounced with increase in actuation potential.

Acknowledgment

The authors acknowledge the Indian Space Research Organisation for their financial support for this research.

References

[1]Cady, W. G., *Piezoelectricity, An Introduction to the Theory and Applications of Electromechanical Phenomena in Crystals*, Vol. 1, Dover, New York, 1964.

[2]Ikeda, T., *Fundamentals of Piezoelectricity*, Oxford Univ. Press, Oxford, 1990.

[3]Eringen, A. C., and Suhubi, E. S., "Non-Linear Theory of Simple Micro-Elastic Solid," *International Journal of Engineering Sciences*, Vol. 2, No. 2, 1964, pp. 189–203.

[4]Tiersten, H. F., "On the Nonlinear Equations of Electro-Thermo-Elasticity," *International Journal of Engineering Sciences*, Vol. 9, No. 7, 1971, pp. 587–604.

[5]Bassiouny, E., Ghaleb, A. F., and Maugin, G. A., "Thermodynamical Formulation for Coupled Electro-Elastic Hysteresis Effects, 1," *International Journal of Engineering Sciences*, Vol. 26, No. 12, 1988, pp. 1279–1295.

[6]Zhang, X. D., and Rogers, C. A., "A Macroscopic Phenomenological Formulation for Coupled Electro-Elastic Effects in Piezoelectricity," *Journal of Intelligent Material Systems and Structures*, Vol. 4, 1993, pp. 307–316.

[7]Crawley, E. F., "Intelligent Structures for Aerospace : A Technological Overview and Assessment," *AIAA Journal*, Vol. 31, No. 8, 1994, pp. 1689–1699.

[8]Zhang, X. D., and Sun, C. T., "Formulation of an Adaptive Sandwich Beam," *Smart Materials and Structures*, Vol. 5, No. 6, 1996, pp. 814–823.

[9]Dube, G. P., Santosh, K., and Dumir, P. C., "Exact Electro-Thermo-Elastic Solution of Simply-Supported Orthotropic Flat Panel in Cylindrical Bending," *International Journal of Mechanical Sciences*, Vol. 38, No. 11, 1996, pp. 1161–1177.

[10]Chattopadhyay, A., Gu, H., and Li, J., "A Coupled Electro-Thermo-Elasticity Theory for Smart Composites Under Thermal Load," *9th International Conference on Adaptive Structures and Technologies*, Technomic, Lancaster, PA, 1998, pp. 156–164.

[11]Aldraihem, J. O., and Ahmed, A. K., "Smart Beams with Extension and Thickness-Shear Piezoelectric Actuators," *Smart Materials and Structures*, Vol. 9, No. 1, 2000, pp. 1–9.

[12]Librescu, L., Meirovitch, L., and Na, S. S., "Control of Cantilever Vibration via Structural Tailoring and Adaptive Materials," *AIAA Journal*, Vol. 35, No. 8, 1997, pp. 1309–1315.

[13]Crawley, E. F., and Luis, J. D., "Use of Piezoelectric Actuators as Elements of Intelligent Structures," *AIAA Journal*, Vol. 25, No. 10, 1987, pp. 1373–1385.

[14]Shen, M-H. H., "Analysis of Beams Containing Piezoelectric Sensors and Actuators," *Smart Materials and Structures*, Vol. 3, No. 4, 1994, pp. 439–447.

[15]Benjeddou, A., Trindade, M. A., and Ohayon, R., "New Shear Actuated Smart Structure Beam Finite Element," *AIAA Journal*, Vol. 37, No. 3, 1999, pp. 378–383.

[16]Robbins, D. N., and Reddy, J. N., "Analysis of Piezoelectrically Actuated Beams Using a Layer-Wise Displacement Theory," *Computers and Structures*, Vol. 41, No. 2, 1991, pp. 265–279.

[17]Ha, S. K., Keilers, C., and Chang, F., "Finite Element Analysis of Composite Structures Containing Distributed Piezoceramic Sensors and Actuators," *AIAA Journal*, Vol. 30, No. 3, 1992, pp. 772–780.

[18]Shih, H., "Distributed Vibration Sensing and Control of a Piezoelectric Laminated Curved Beam," *Smart Materials and Structures*, Vol. 9, No. 6, 2000, pp. 761–766.

[19]Liu, G. R., Peng, X. Q., and Lam, K. Y., "Vibration Control Simulation of Laminated Composite Plates with Integrated Piezoelectrics," *Journal of Sound and Vibration*, Vol. 220, No. 5, 1999, pp. 827–846.

[20]Sun, B., and Huang, D., "Analytical Vibration Suppression Analysis of Composite Beams with Piezoelectric Laminae," *Smart Materials and Structures*, Vol. 9, No. 6, 2000, pp. 751–760.

[21]Tzou, H. S., and Howard, R. V., "A Piezo-Thermo-Elastic Thin Shell Theory Applied to Active Structures," *Journal of Vibrations and Acoustics*, Vol. 116, No. 3, 1994, pp. 295–302.

[22]Mujumdar, P., Seth, B., and Seshu, P., "Experiments on Piezoelectric Bimorph Actuator Element (Bending Motor)," Dept. of Aerospace Engineering, ARDB-SP-TR-2000-945-01, Indian Inst. of Technology, Bombay, India, Feb. 2000.

[23]Chopra, I., "Status of Application of Smart Structures Technology to Rotor-craft Systems," *Proceedings of International Seminar on Aerospace Opportunities: Trends and Technologies*, Aeronautical Society of India, Bangalore, India, 1998.

[24]Venkatesan, C., and Upadhyay, C. S., "A General Approach to Modeling and Analysis of Smart Structures," *Proceedings of ISSS–SPIE 2002 International Conference on Smart Materials, Structures and Systems*, Microart Multimedia Solutions, Bangalore, India, 2002, pp. 163–174.

[25]Sahu, P., "Analysis of a Smart Beam Structure," B.Tech. Project Rept., Dept. of Aerospace Engineering, Indian Inst. of Technology Kanpur, India, July 2001.

K. Shivakumar
Associate Editor